

A nuclear disc at Cosmic Noon: evidence of early bar-driven galaxy evolution

Zoe A. Le Conte,¹★ Dimitri A. Gadotti,¹ Thomas Harvey,² Leonardo Ferreira,³ Christopher J. Conselice,² Taehyun Kim,⁴ Camila de Sá-Freitas,⁵ Francesca Fragkoudi,⁶ Justus Neumann,⁷ and E. Athanassoula⁸

¹Centre for Extragalactic Astronomy, Department of Physics, Durham University, South Road, Durham DH1 3LE, UK

²Jodrell Bank Centre for Astrophysics, University of Manchester, Oxford Road, Manchester M13 9PL, UK

³Instituto de Matemática Estatística e Física, Universidade Federal do Rio Grande, Rio Grande, RS, Brazil

⁴Department of Astronomy and Atmospheric Sciences, Kyungpook National University, Daegu, 41566, Republic of Korea

⁵European Southern Observatory, Alonso de Córdova 3107, Vitacura, Región Metropolitana, Chile

⁶Institute for Computational Cosmology, Department of Physics, Durham University, South Road, Durham DH1 3LE, UK

⁷Max-Planck-Institut für Astronomie, Königstuhl 17, D-69117 Heidelberg, Germany

⁸Aix Marseille Univ, CNRS, CNES, LAM, Marseille, France

Accepted XXX. Received YYY; in original form ZZZ

ABSTRACT

Recent studies have revealed that bars can form as early as a few billion years after the Big Bang, already displaying similar characteristics of evolved bars in the Local Universe. Bars redistribute angular momentum across the galaxy, regulating star formation, AGN activity, and building new stellar structures such as nuclear discs. However, the effects of bar-driven evolution on young galaxies are not yet known, as no evidence of bar-built stellar structures has ever been found beyond $z = 1$, until now. In this work, we show evidence of a bar-built, star-forming nuclear disc, already present at redshift $z = 1.5$. This is the first evidence of a bar-built stellar structure at Cosmic Noon. We find that this nuclear disc is actively forming stars and has the same size as some nuclear discs in nearby galaxies. This evidence solidifies the now emerging picture in which bars are fundamental not only in the late evolution of galaxies, but also in their early evolutionary stages. It changes the current paradigm by urging a revision of our picture of galaxy evolution beyond redshift one, to include new considerations on the role played by bars as early as a few billion years after the Big Bang.

Key words: galaxies: evolution – galaxies: structure – galaxies: high-redshift

1 INTRODUCTION

Studies of barred galaxies at redshifts $z > 1$ have become prevalent in the past few years, thanks to the improved sensitivity and infrared coverage of the James Webb Space Telescope (JWST). These studies have revealed that bars, which are the key drivers of internal evolution in disc galaxies, can form as early as a few billion years after the Big Bang (e.g., Le Conte et al. 2024; Guo et al. 2023, 2025; Géron et al. 2025). At Cosmic Noon, these bars are found to be as long as the bars in local disc galaxies (e.g., Le Conte et al. 2026). These surprising results suggest a rapid evolution of bars when the Universe was still young (e.g., Kalita et al. 2025). Bars redistribute angular momentum, as well as baryonic and dark matter, regulate star formation and AGN activity, and build new stellar structures such as nuclear discs (e.g., Coelho & Gadotti 2011; Donohoe-Keyes et al. 2019; Gadotti et al. 2020; Silva-Lima et al. 2022; Garland et al. 2024, and references therein).

Nuclear discs are considered ubiquitous in local barred galaxies and range in size and properties (e.g., Erwin 2004; Comerón et al. 2010, see also Schultheis et al. (2025) for a review). The size of the

nuclear disc is on the order of 100s of parsecs in radius, and is a rapidly rotating structure at the centre of the barred galaxy, separate from the main galaxy disc. As such, nuclear discs have properties contrasting to those of classical bulges, and the two structures appear in nearby galaxy observations at least as frequently (e.g., Bittner et al. 2020; Fraser-McKelvie et al. 2025). A nuclear disc is thought to be formed by the bar funnelling gas towards the centre, and acts as a reservoir for gas; thus, showing heightened star formation (e.g., Bittner et al. 2020). The nuclear disc size is limited by the inner Lindblad resonances (ILR) of the bar potential (Shlosman et al. 1989), and recent studies have reported on the relation that nuclear discs in the local Universe are $\sim 13\%$ of their bar lengths (Gadotti et al. 2020). The nuclear disc is an indicator that bar-driven galaxy evolution has commenced and is effectively redistributing angular momentum. Moreover, it creates a stable environment for further gas funnelling toward the central supermassive black hole, and potentially fueling AGN. Further gas inflow is achieved by the formation of non-axisymmetric nuclear substructures in the nuclear disc, such as a nuclear bar or spiral arms. The impact of bars and the occurrence of nuclear discs during Cosmic Noon are yet to be explored, due to spatial resolution limitations (see discussion in Gadotti 2026).

In this Letter, we perform detailed structural analyses in JWST

★ E-mail: zoe.a.le-conte@durham.ac.uk

images of barred galaxies to present evidence of a nuclear disc in a barred galaxy at a spectroscopic redshift of $z = 1.5$. This is the most distant nuclear disc to date. In the next section, we present the data and analyses performed, while in § 3 we present the results, which are discussed in § 4. Section 5 summarises our main conclusions. We adopt the Planck 2020 cosmological parameters for a flat Λ CDM cosmology with $H_0 = 67.36$, $\Omega_m = 0.3153$, and $\Omega_\Lambda = 0.6847$ (Planck Collaboration et al. 2020).

2 DATA ANALYSIS

2.1 Data

For this study, we utilise public JWST observations from the Cosmic Evolution Early Release Science Survey (CEERS; PI: Filkelstein, ID=1345, Finkelstein et al. 2023). These observations included imaging from the Near Infrared Camera (NIRCam) filters (F115W, F150W, F200W, F277W, F356W, F410M, and F444W) and spectra from the Near Infrared Spectrograph (NIRSpec) with medium resolution, $R \sim 1,000$, and gratings (G140M, G235M, and G395M). The NIRCam exposures we retrieved from the Mikulski Archive for Space Telescopes (MAST) and reprocessed with the official JWST pipeline (v1.8.2, CRDS v1084), following the procedures of Ferreira et al. (2023) and Adams et al. (2023) but incorporating several refinements which are summarised in Le Conte et al. (2026). To ensure sub-pixel alignment across the dataset, each filter is re-projected onto the F444W grid at $0.03''/\text{pixel}^{-1}$. A comprehensive description of the workflow and its validation is given in Adams et al. (2024); Conselice et al. (2024); Harvey et al. (2025b). We thus produce 30 mas 128x128 pixel cutouts from the NIRCam data.

We use the spectroscopic redshifts from CEERS. In this study, we use the NIRCam empirical Point Spread Function (PSF) Full Width Half Maximum (FWHM)¹. The F115W PSF FWHM is $0.040''$; corresponding to a linear resolution of 0.347 kpc for $z = 1.461$. The PSF FWHM degrades for longer wavelength filters; hence, the F444W PSF FWHM is $0.145''$ with a linear resolution of 1.259 kpc.

2.2 Unsharp masking

Bright components at the centre of galaxies can make it difficult to identify finer substructures, such as the nuclear disc. The change in light between the nuclear disc and the stellar bar or main disc can be enhanced by the effective technique of unsharp masking (e.g., Malin 1977), which removes light associated with large structures in the galaxy. We generate unsharp masked images by first convolving the NIRCam image with a circular Gaussian kernel with $\sigma = 3$ pixels, corresponding to $0.09''$. The kernel size was chosen to be greater than $2 \times \text{FWHM}$ and the radius of a possible nuclear disc. The original NIRCam image is then divided by the convolved image to reveal small structures in the galaxy.

2.3 Photometric decompositions

A powerful technique for deriving the structural properties of a galaxy is to perform a two-dimensional photometric decomposition, for which here we use IMFIT v1.8 (Erwin 2015). We prepared the NIRCam images for IMFIT employing SExtractor (Bertin &

Arnouts 1996) to create masks of neighbouring sources. Additionally, we convert the pixel units of the NIRCam images from MJy/sr to DN/s by dividing the image by the FLUXCONV constant from the image header. We edit the IMFIT configuration file to have the corresponding gain, readout noise, subtracted background, and exposure time for each NIRCam filter. The galaxy centre is defined as the brightest pixel and has an upper and lower bound of ± 2 pixels. The fitted structural components are centred on the galaxy centre. We fed IMFIT with simulated NIRCam PSFs generated by the STPSF package (Perrin et al. 2014). We selected a region of ± 20 pixels centred on the galaxy to convolve with a four-fold oversampled PSF, and we chose the Differential Evolution (DE) algorithm (Storn & Price 1997) to minimise the fit statistic and find the best-fit model. The algorithm does not require an initial guess for parameter values; rather, it requires upper and lower limits, which makes it less likely to be trapped in local minima (for a discussion on the robustness of the DE algorithm, see Gadotti 2026).

We fit all NIRCam images with three components. The radial light/mass profile of the disc is described by an exponential; a generalised Sérsic function describes the bar; a Sérsic function describes the central component. Collectively, we fit 18 free parameters. As a result, we have a component model defined by concentric and homologous ellipses of position angle PA and ellipticity ϵ , defined by

$$\epsilon = 1 - \frac{b}{a}, \quad (1)$$

where b is the length of the semi-minor axis and a is the length of the semi-major axis of the ellipse. The intensity for a given ellipse in the central component is defined as:

$$I(r) = I_e \exp(-b_n[(\frac{r}{r_e})^{1/n} - 1]), \quad (2)$$

where I_e is the intensity at the effective radius r_e , n is the Sérsic index and b_n is a constant that is a function of n . We use these models to obtain the structural parameters of the different galactic components, such as characteristic sizes and Sérsic index, as well as luminosity/mass fractions. In addition, we subtract the combined models from the original NIRCam image to create a residual image that enhances stellar structures not modelled.

2.4 Isophotal analysis

Structures in galaxies can also be traced with contours of equal intensity, i.e., isophotes. The structures deduced from isophotal contours can be parameterised with ellipse fitting. For example, an indication of a barred nuclear disc within a barred galaxy is a double peak in the radial profile of the ellipticity of the isophotes (see Erwin 2004).

We use `photutils.isophote` from Python's astropy package (e.g., Bradley et al. 2022) to fit elliptical isophotes to the NIRCam images. Firstly, we run this module with the galaxy centre coordinates as free parameters, and iterate through the initial parameters to obtain the best fit. The module assesses a 10×10 window centred around a specified point for each isophote to get a central coordinate. Then, we select isophotes of radius $10 - 40\%$ of the whole galaxy, and determine the galaxy centre to be the average of their central coordinates. Finally, the isophotal ellipse fitting is repeated, however, with a fixed centre.

We obtain the parameters of the fitted ellipses at increasing radii, and we are most interested in the radial profiles of the ellipticity of the isophotes. We thus focus on finding the semi-major axis of any major and isolated ellipticity peaks.

¹ JWST user documentation: <https://jwst-docs.stsci.edu/jwst-near-infrared-camera/nircam-performance/nircam-point-spread-functions>

2.5 SED fitting

We perform resolved SED fitting using the Bayesian SED fitting tool `BAGPIPES` (e.g., Carnall et al. 2018) via the `EXPANSE` package (e.g., Harvey et al. 2025a) in order to produce resolved measurements of the stellar mass and star formation rate surface densities in the central component, bar, and disc of the galaxy. Our SED fitting model is constructed as follows: we fix the redshift to the known spectroscopic redshift, with the flexible non-parametric ‘continuity’ star formation history (SFH) of Leja et al. (2019). To model dust attenuation, we use a single-component dust law (Calzetti et al. 2000), with a uniform prior of $0 \leq A_V \leq 5$. We utilise a BPASS (Stanway & Eldridge 2018) SPS model, with a Kroupa (2001) initial mass function (IMF), allowing for nebular emission from star-forming regions using CLOUDY post-processing with a uniform prior on the logarithm of the ionisation parameter $\log U$ between -4 and -1. We allow a broad log-uniform prior on stellar metallicity, between 10^{-3} and $2.5Z_\odot$.

Our resolved SED fitting process broadly follows Harvey et al. (2025a); in short, we convolve all NIRCam cutouts to the measured PSF for the F444W filter using an empirical PSF model, then perform Voronoi binning on the F277W cutout using `VORBIN` (Cappellari & Copin 2012) to ensure a per-bin $\text{SNR} > 10$ in every fitted region. We mask a small number of bins very close to the detector edge in the long wavelength filters, which are noise-dominated. We fit each bin independently using `BAGPIPES` as described above using MultiNest nested sampling (e.g., Feroz et al. 2009). We thus produce maps of star formation rate (SFR) density, stellar mass density and the strength of the 4000Å break (D4000), which correspond to the 50th percentile of the posterior distribution for each bin and parameter.

3 RESULTS

Armed with the analysis tools described above, we studied the structural properties of a subset of barred galaxies at $z > 1$ from the work presented in Le Conte et al. (2026). The study found over 70 barred galaxies via visual classification, and the analysis techniques described here were used to measure the bar properties. In the course of these analyses, we have found one galaxy (CEERS-4031) with evidence of the presence of a nuclear disc.

We thus report here the discovery of the first nuclear disc observed beyond $z = 1$ and having an age of only 4.5 billion years after the Big Bang. The $\log_{10}(M_\star) = 10.75 \pm 0.05 M_\odot$ galaxy was categorised as a strongly barred galaxy in our study of the bar fraction (e.g., Le Conte et al. 2026), which used visual classification and ellipse fits to identify a high-redshift sample of barred galaxies and measure their properties. This galaxy already stood out in that analysis, as we measured a long bar with length (semi-major axis) $L_{\text{bar}} = 5.33 \text{ kpc}$ in a near face-on spiral disc.

Figure 1 shows the galaxy in seven NIRCam filters, where a central structure is already discernible; in particular, an elongated structure is seen in the bluest filters (which have better spatial resolution). The NIRCam filter wavelength range spans from $1.15\mu\text{m}$ to $4.44\mu\text{m}$, corresponding to a rest-frame wavelength of $0.47\mu\text{m}$ to $1.80\mu\text{m}$ for this galaxy at $z = 1.461$. The RGB image, constructed using images from the shorter-wavelength channel, reveals that the ends of the elongated central stellar structure are bluer, indicating younger stellar populations and enhanced star formation.

Using three of the techniques described in detail in § 2, encompassing structure-enhancement and model-dependent approaches, we reveal the nature of the nuclear structure. These techniques are: unsharp

masking, which enhances high spatial frequency substructures; 2D photometric decomposition, which involves the fitting of a three-component model composed of a disc, bar, and a central component representing the main stellar structures of the galaxy; and isophotal ellipse fitting to the isoluminance contours of the image, allowing one to obtain a radial ellipticity profile of the galaxy and its inner components. The photometric decomposition can also be used to produce residual images, often revealing substructures.

The results from these analyses are shown in Fig. 2. An elongated structure exhibiting a pair of symmetric ‘wings’ resembling spiral arms $\approx 1.3 \text{ kpc}$ in radius, is enhanced in the unsharp-marked images. These images reveal a distinctive light deficit between the bar and this central stellar structure. The light deficit is important because it indicates a physical separation between the central stellar structure and bar, and thus, not simply a continuation of the bar towards the centre.

The stellar substructure is further highlighted in the residuals of the multi-component fit to the image. For the NIRCam filters, F150W and F200W, we subtract the optimised model from the original image, now clearly revealing a spiral structure. Again, the nuclear spiral structure consists of two winding arms that extend to $\approx 1.3 \text{ kpc}$. In F200W, the 2D decompositions indicate a central component with an effective radius, $R_e \approx 0.5 \text{ kpc}$, and with a Sérsic index, $n = 0.8$. The near-exponential radial profile of the central component strongly suggests that it is indeed a nuclear disc hosting nuclear spiral arms, much like nearby counterparts such as NGC 1097 and NGC 4314 (see Erwin & Sparke 2003; Gadotti et al. 2019; Gadotti 2026).

In addition, the elongated central structure from which the nuclear spiral arms emerge, readily seen in the NIRCam images taken with the bluest filters, suggests that the nuclear disc also hosts a nuclear bar. An indication of a barred nuclear disc within a nearby barred galaxy is shown as a double peak in the radial ellipticity profile derived from ellipse fits, since the two bars produce independent ellipticity peaks. Indeed, we do observe this behaviour in the NIRCam F150W and F200W filters. The peak in ellipticity occurs at a similar radius in both filters, differing by only $\approx 81 \text{ pc}$, and suggests that the nuclear bar has a length of 1050 pc . The shorter wavelength F150W filter indicates a slightly higher ellipticity for the nuclear and main bars than in the F200W filter. Such an effect has also been seen in local barred galaxies (e.g., Menéndez-Delmestre et al. 2024). The nuclear disc itself is slightly larger than the nuclear bar, as seen often in nearby galaxies. In the two approaches that we have conducted, the measurements agree that the nuclear disc size is approximately 1.3 kpc . We list the structural properties of the nuclear disc derived from our analyses along with the host galaxy properties in Table 1.

In local galaxies, the outer parts of nuclear discs are often regions of heightened star formation and younger stellar populations, because gas is driven by the bar towards the centre (see also Huang et al. 2025). To examine whether the area we have identified as the nuclear disc exhibits this characteristic, we perform a resolved Spectral Energy Distribution (SED) fitting and produce property maps, shown in Fig. 3, observing a high SFR density within $R_{\text{ND}} = 1.3$. Additionally, we find very low D4000 values within R_{ND} , indicating younger star-forming populations. This enhanced star formation in the nuclear disc qualitatively agrees with the observed bluer ends of the nuclear bar and nuclear spiral arms in the RGB image in Figure 1. Altogether, we have found that the nuclear structure seen in this galaxy displays similar properties to those of star-forming nuclear discs in the local Universe.

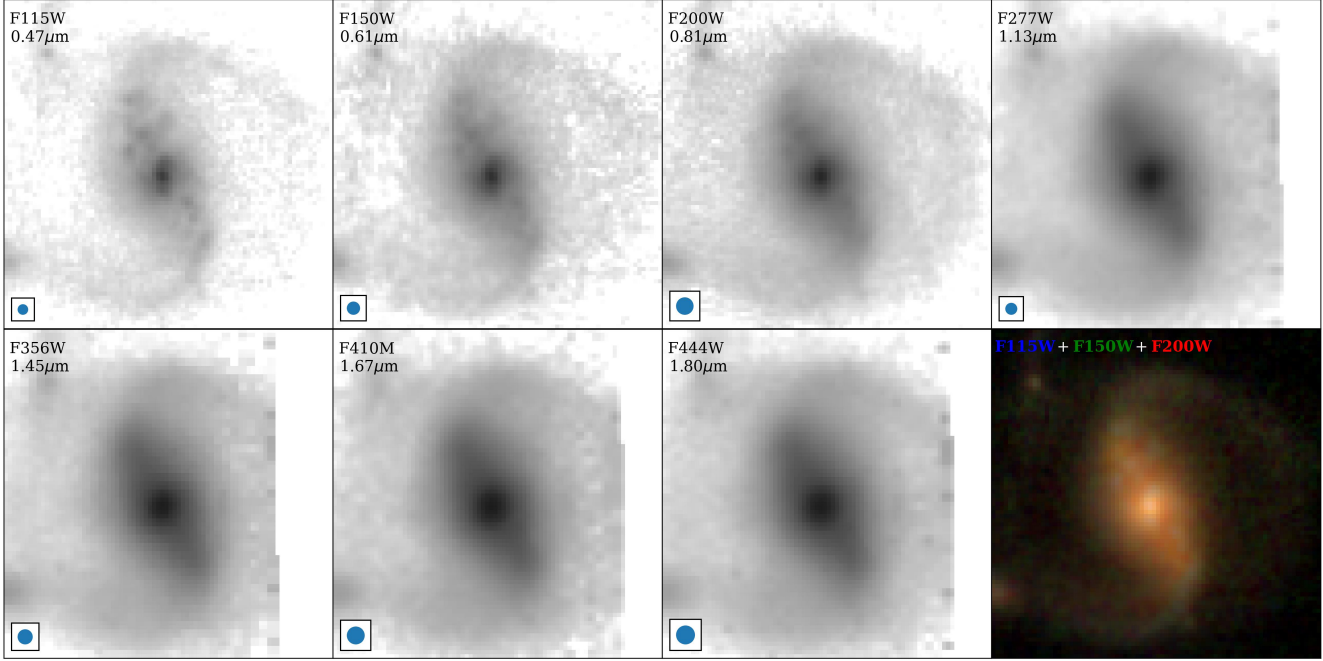


Figure 1. The galaxy images from seven NIRCam filters, annotated in the top-left corner of each image with the filter name and rest-frame wavelength for a redshift of $z = 1.461$. A circle depicting $2 \times \text{FWHM}$ of the PSF is shown in the lower-left corner of each image. The lower-right panel is an RGB image obtained from the filters F115W, F150W and F200W.

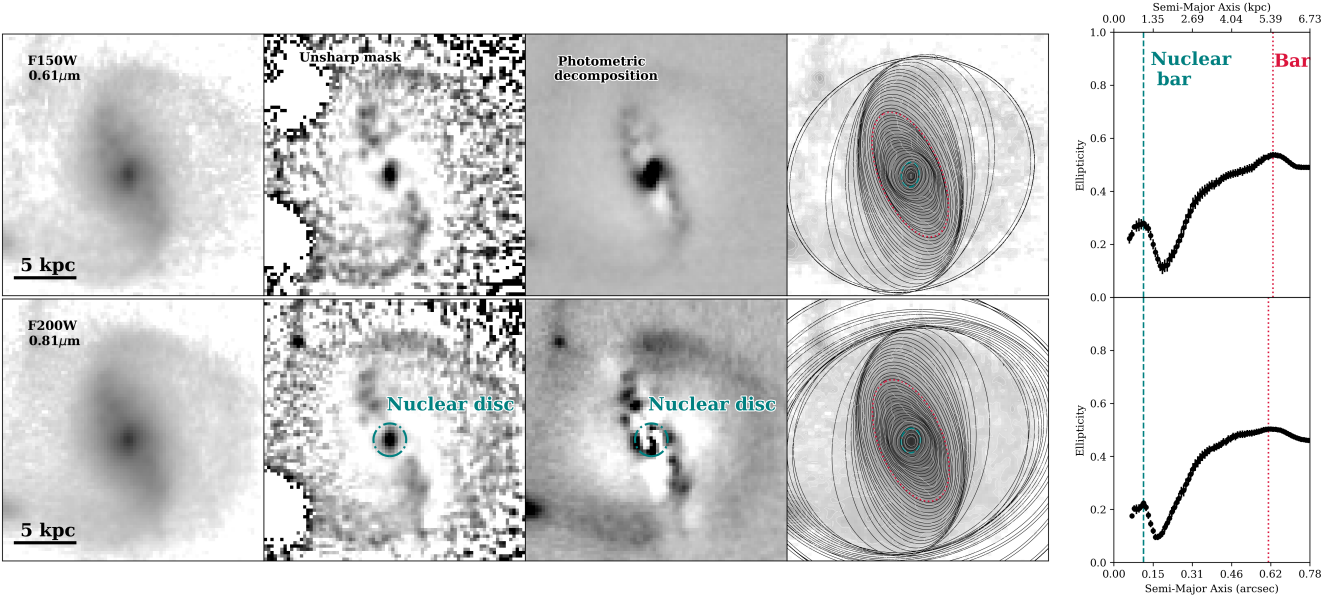


Figure 2. Image analysis of the galaxy in the F150W (top row) and F200W (bottom row) NIRCam filters. From left to right: NIRCam image; unsharp masked image; IMFIT residual image for a multi-component fit; isophotal ellipse fitting of the NIRCam image; ellipticity radial profile from ellipse fitting, showing the peak in ellipticity of the nuclear bar in the nuclear disc as a dashed line and of the main bar as a dotted line. The nuclear disc size, measured with visual inspection of the images, is shown as a dot-dashed circle in the unsharp masked and residual images.

4 DISCUSSION

In studies concerning nearby galaxies, the size of the nuclear disc correlates with the length of the bar (e.g., [Seo et al. 2019](#); [Gadotti et al. 2020](#)), i.e., a larger nuclear disc resides in a longer bar. As the bar drives gas inwards, the nuclear disc is believed to grow inside-out, since the gas halts at successively larger radii, inducing bursts

of star formation always more pronounced at the edge of the nuclear disc (e.g., [Bittner et al. 2020](#)). This is supported by the work of [Kim et al. \(2012\)](#), which finds the higher angular momentum gas at the outer edge of the galaxy to halt at larger radii when funnelled towards the centre by the bar. In this study, we discover a large nuclear disc, $R_{\text{ND}} \approx 1 \text{ kpc}$ and a long bar $\approx 5 \text{ kpc}$, which sits above the nuclear

Property	Value	Unit
RA	214.937795	°
DEC	52.826470	°
Redshift (z)	1.461	
Stellar mass ($\log_{10} M_\star$) ^a	10.75 ± 0.05	M_\odot
Bar length (L_{bar}) ^b	5.33	kpc
Bar ellipticity (e_{bar}) ^b	0.50	
Nuclear bar size (L_{NB}) ^c	1050	pc
Nuclear disc size (R_{ND}) ^d	1300	pc
Nuclear disc effective radius (R_e) ^e	525	pc
Nuclear disc Sérsic index (n) ^e	0.843	
Disc-total luminosity ratio (D/T) ^e	0.50	
Bar-total luminosity ratio (B/T) ^e	0.33	
Nuclear disc-total luminosity ratio (ND/T) ^e	0.17	

Table 1. Main properties of CEERS-4031.

^a From photometry.

^b From ellipse fits in F200W (see Le Conte et al. 2026).

^c From ellipse fits in F200W (see Figure 2).

^d From visual inspection of the unsharp-masked images and decomposition residuals in F200W. Both measurements agree on the quoted value.

^e From the photometric decomposition in F200W.

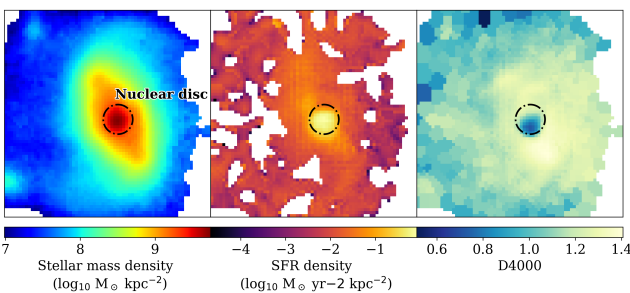


Figure 3. Resolved property maps from NIRCam SED fitting. Left to right: stellar mass density, SFR density, and the strength of the 4000Å break.

disc size to bar length relation in Gadotti et al. (2020). Shlosman et al. (1989) define the co-evolution of the nuclear disc and bar to be limited by the Inner Lindblad Resonance (ILR) at $0.1R_{bar}$. Here, we find a greater radius at $0.2R_{bar}$, suggesting that the nuclear disc has grown significantly and rapidly, implying a substantial bar-driven gas inflow that may be connected to earlier AGN activity.

We also identify nuclear spiral arms and a nuclear bar within the nuclear disc. Our result is supported by the theoretical work of Kim et al. (2012), which finds nuclear spiral arms to be present in nuclear discs of type x_2 and $R_{ND} > 0.6$ kpc. In the local Universe, up to $\approx 50\%$ of the galaxies with stellar mass $\log_{10}(M_\star) > 10.5 M_\odot$ (which corresponds to the galaxy in this study) host a nuclear bar (e.g., Erwin 2024).

A novel approach to age dating the bar of nearby disc galaxies is developed in de Sá-Freitas et al. (2023, 2025), where the authors predict that both bars and nuclear discs might be present since $z \sim 4$. The method assumes that the nuclear disc forms quickly after the bar, so differences in the star-formation histories of the nuclear disc and the main disc reflect the age of the bar. Until now, nuclear discs have been found only in nearby galaxies, and the assumption that nuclear discs form relatively fast after the stellar bar was supported by simulations. Our discovery of a nuclear disc in a high-redshift galaxy is evidence that nuclear discs can form at early epochs, in

particular, during the epoch of bar formation. To understand the star formation history of this galaxy and disentangle the age of the bar, we would require NIRSpec IFU data.

This study focuses on the discovery of one nuclear disc in a barred galaxy; however, this motivates the need for a nuclear disc population study beyond the local Universe. Barred galaxies are ubiquitous out to Cosmic Noon (e.g., Walmsley et al. 2025; Géron et al. 2025; Espejo Salcedo et al. 2025), and if the occurrence of nuclear discs in nearby barred galaxies can be projected to higher redshifts (e.g., de Sá-Freitas et al. 2023, 2025), then we might be able to detect many more of the largest nuclear discs with JWST. Population statistics will improve our understanding of the environments which promote bar-driven evolution and unveil the role of nuclear discs in AGN fueling during the peak of cosmic AGN activity.

5 CONCLUSIONS

We discover the most distant nuclear disc within a barred galaxy to date, at $z = 1.461$, implying unequivocal evidence for bar-driven galaxy evolution during early epochs. The nuclear disc has a radius of $R_{ND} \approx 1$ kpc, hosts a nuclear bar and nuclear spiral arms, and shows a near-exponential radial profile, thus being overall consistent with nuclear discs residing in nearby galaxies. Within the nuclear disc region, we observe heightened star formation and younger stellar populations, indicating bar-driven gas inflow. This nuclear disc thus shows all the hallmark signatures of bar-driven evolution in nearby galaxies and is evidence of the fast maturing of galaxy discs and bars at Cosmic Noon.

ACKNOWLEDGEMENTS

This work was supported by STFC grants ST/X508354/1, ST/T000244/1 and ST/X001075/1. This work used the DiRAC@Durham facility managed by the Institute for Computational Cosmology on behalf of the STFC DiRAC HPC Facility (www.dirac.ac.uk). The equipment was funded by BEIS capital funding via STFC capital grants ST/K00042X/1, ST/P002293/1, ST/R002371/1 and ST/S002502/1, Durham University, and STFC operations grant ST/R000832/1. DiRAC is part of the National e-Infrastructure. TK is supported by Basic Science Research Program through the National Research Foundation of Korea (NRF) funded by the Ministry of Education (RS-2025-25399934).

DATA AVAILABILITY

The specific observations analysed can be accessed via <https://doi.org/10.17909/xm8m-4t59>. This work used ASTROPY (Astropy Collaboration et al. 2013), SExtractor (Bertin & Arnouts 1996), PHOTUTILS (Bradley et al. 2022), IMFIT (Erwin 2015) and EXPANSE (e.g., Harvey et al. 2025a).

REFERENCES

- Adams N. J., et al., 2023, *MNRAS*, 518, 4755
- Adams N. J., et al., 2024, *ApJ*, 965, 169
- Astropy Collaboration et al., 2013, *A&A*, 558, A33
- Bertin E., Arnouts S., 1996, *A&AS*, 117, 393
- Bittner A., et al., 2020, *A&A*, 643, A65

Bradley L., et al., 2022, astropy/photutils: 1.5.0, doi:10.5281/zenodo.6825092, <https://doi.org/10.5281/zenodo.6825092>

Calzetti D., Armus L., Bohlin R. C., Kinney A. L., Koornneef J., Storchi-Bergmann T., 2000, *ApJ*, **533**, 682

Cappellari M., Copin Y., 2012, Astrophysics Source Code Library, pp ascl-1211

Carnall A., McLure R., Dunlop J., Davé R., 2018, Monthly Notices of the Royal Astronomical Society, 480, 4379

Coelho P., Gadotti D. A., 2011, *ApJ*, **743**, L13

Comerón S., Knapen J. H., Beckman J. E., Laurikainen E., Salo H., Martínez-Valpuesta I., Buta R. J., 2010, *MNRAS*, **402**, 2462

Conselice C. J., et al., 2024, *MNRAS*, **531**, 4857

Donohoe-Keyes C. E., Martig M., James P. A., Kraljic K., 2019, *MNRAS*, **489**, 4992

Erwin P., 2004, *A&A*, **415**, 941

Erwin P., 2015, *ApJ*, **799**, 226

Erwin P., 2024, *MNRAS*, **528**, 3613

Erwin P., Sparke L. S., 2003, *ApJS*, **146**, 299

Espejo Salcedo J. M., et al., 2025, arXiv e-prints, p. arXiv:2503.21738

Feroz F., Hobson M., Bridges M., 2009, Monthly Notices of the Royal Astronomical Society, 398, 1601

Ferreira L., et al., 2023, *ApJ*, **955**, 94

Finkelstein S. L., et al., 2023, *ApJ*, **946**, L13

Fraser-McKelvie A., et al., 2025, *A&A*, **700**, A237

Gadotti D. A., 2026, *MNRAS*, **545**, staf2072

Gadotti D. A., et al., 2019, *MNRAS*, **482**, 506

Gadotti D. A., et al., 2020, *A&A*, **643**, A14

Garland I. L., et al., 2024, *MNRAS*, **532**, 2320

Guo Y., et al., 2023, *ApJ*, **945**, L10

Guo Y., et al., 2025, *ApJ*, **985**, 181

Géron T., et al., 2025, Galaxy Zoo CEERS: Bar fractions up to $z \approx 4.0$ (arXiv:2505.01421), <https://arxiv.org/abs/2505.01421>

Harvey T., et al., 2025a, Monthly Notices of the Royal Astronomical Society, **542**, 2998

Harvey T., et al., 2025b, *ApJ*, **978**, 89

Huang S., Kawabe R., Umehata H., Kohno K., Tamura Y., Saito T., 2025, *Nature*, **641**, 861

Kalita B. S., et al., 2025, *ApJ*, **979**, L44

Kim W.-T., Seo W.-Y., Kim Y., 2012, *ApJ*, **758**, 14

Kroupa P., 2001, Monthly Notices of the Royal Astronomical Society, **322**, 231

Le Conte Z. A., et al., 2024, *MNRAS*, **530**, 1984

Le Conte Z. A., et al., 2026, *MNRAS*, **545**, staf2010

Leja J., Carnall A. C., Johnson B. D., Conroy C., Speagle J. S., 2019, The Astrophysical Journal, **876**, 3

Malin D. F., 1977, AAS Photo Bulletin, **16**, 10

Menéndez-Delmestre K., et al., 2024, *MNRAS*, **527**, 11777

Perrin M. D., Sivaramakrishnan A., Lajoie C.-P., Elliott E., Pueyo L., Ravindranath S., Albert L., 2014, in Oschmann Jr. J. M., Clampin M., Fazio G. G., MacEwen H. A., eds, Society of Photo-Optical Instrumentation Engineers (SPIE) Conference Series Vol. 9143, Space Telescopes and Instrumentation 2014: Optical, Infrared, and Millimeter Wave. p. 91433X, doi:10.1117/12.2056689

Planck Collaboration et al., 2020, *A&A*, **641**, A6

Schultheis M., Sormani M. C., Gadotti D. A., 2025, *A&ARv*, **33**, 7

Seo W.-Y., Kim W.-T., Kwak S., Hsieh P.-Y., Han C., Hopkins P. F., 2019, *ApJ*, **872**, 5

Shlosman I., Frank J., Begelman M., 1989, *Nature*, 338

Silva-Lima L. A., Martins L. P., Coelho P. R. T., Gadotti D. A., 2022, *A&A*, **661**, A105

Stanway E. R., Eldridge J., 2018, Monthly Notices of the Royal Astronomical Society, **479**, 75

Storn R., Price K., 1997, *Journal of Global Optimization*, 11

Walmsley M., et al., 2025, Euclid Quick Data Release (Q1): First visual morphology catalogue (arXiv:2503.15310), <https://arxiv.org/abs/2503.15310>

de Sá-Freitas C., et al., 2023, *A&A*, **671**, A8

de Sá-Freitas C., et al., 2025, arXiv e-prints, p. arXiv:2503.20864

This paper has been typeset from a TeX/LaTeX file prepared by the author.